

Shot-noise and differential conductance as signatures of putative topological superconductivity in $\text{FeSe}_{0.45}\text{Te}_{0.55}$

Ka Ho Wong¹, Eric Mascot¹, Vidya Madhavan², Dale J. Van Harlingen², and Dirk K. Morr¹

¹ *University of Illinois at Chicago, Chicago, IL 60607, USA*

² *University of Illinois at Urbana Champaign, Champaign, IL 61801, USA*

(Dated: October 7, 2021)

We present a theory for the differential shot noise, dS/dV , as measured via shot-noise scanning tunneling spectroscopy, and the differential conductance, dI/dV , for tunneling into Majorana zero modes (MZMs) in the putative topological superconductor $\text{FeSe}_{0.45}\text{Te}_{0.55}$. We demonstrate that for tunneling into chiral Majorana edge modes near domain walls, as well as MZMs localized in vortex cores and at the end of defect lines, dS/dV vanishes whenever dI/dV reaches a quantized value proportional to the quantum of conductance. These results are independent of the particular orbital tunneling path, thus establishing a vanishing dS/dV concomitant with a quantized dI/dV , as universal signatures for Majorana modes in two-dimensional topological superconductors, irrespective of the material's specific complex electronic bandstructure.

Introduction The unambiguous experimental identification of Majorana zero modes (MZMs) in topological superconductors, the putative building blocks for topological quantum computing, has remained a major challenge. While it has been predicted that the differential conductance, dI/dV , for tunneling into MZMs is quantized both for one-dimensional [1, 2] and two-dimensional topological superconductors [3], and that the shot-noise associated with the tunneling into Majorana modes exhibits various characteristic signatures [1, 4–10], the experimental verification of these predictions has remained difficult due to the close proximity of trivial in-gap states, as well as small superconducting gaps. Recent experiments, however, have provided enthralling evidence for the existence of topological surface superconductivity in the iron-based superconductor $\text{FeSe}_{0.45}\text{Te}_{0.55}$ possessing a full s_{\pm} -wave gap of a few meV. In particular, these experiments have reported the existence of a surface Dirac cone [11], of MZMs in the vortex core [12–14] and at the end of line defects [15] in monolayer $\text{FeSe}_{0.45}\text{Te}_{0.55}$, and of a Majorana edge mode at a domain wall [16]. While the physical origin of this putative topological phase has remained a question of debate, either being ascribed to the existence of a topological insulator whose surface Dirac cone is gapped out by proximitized superconductivity [11, 17], or to the interplay [18] of an s_{\pm} -wave gap, a Rashba spin-orbit interaction and recently observed surface ferromagnetism [19, 20], the question naturally arises of what type of universal physical observables associated with the existence of localized MZMs or chiral Majorana edge modes can be expected in the multi-orbital $\text{FeSe}_{0.45}\text{Te}_{0.55}$ compound.

The development of scanning tunneling shot-noise spectroscopy [21–25] has opened a new approach to investigating this question as it allows the direct measurement of the local shot-noise associated with electron tunneling into a Majorana mode, thus complementing the measurement of the differential conductance. Using a Keldysh Greens function approach, we compute the dif-

ferential shot noise, dS/dV , and differential conductance, dI/dV , using a recently proposed 5-orbital model for $\text{FeSe}_{0.45}\text{Te}_{0.55}$ in which the topological superconducting phase arises from the interplay of surface magnetism, a Rashba spin-orbit interaction, and a hard superconducting gap with s_{\pm} -symmetry [18]. Specifically, we study dS/dV and dI/dV for three different occurrences of Majorana modes: a chiral Majorana edge mode at a domain wall, and MZMs in vortex cores and at the end of line defects. We demonstrate that for each of these cases, the electron tunneling into a Majorana mode is accompanied by a vanishing differential shot noise, dS/dV , and a quantized differential conductance, dI/dV , being equal to the quantum of conductance. Since these results hold for tunneling into each of the 5 relevant orbitals, they demonstrate that a quantized dI/dV , and a vanishing dS/dV are universal signatures for Majorana modes in two-dimensional topological superconductors, that are independent of the material's specific complex electronic bandstructure. This, in turn, allows one to employ the vanishing of the differential shot noise as a local marker to detect topological phase transitions. Finally, we show that the measurement of a non-vanishing supercurrent along a domain wall using a Scanning SQUID (superconducting quantum interference device) Microscope (SSM) [26] is a third characteristic feature for the existence of Majorana modes, thus complementing those features found in dS/dV and dI/dV . The combination of our results points toward new possibilities for the experimental identification of Majorana modes in complex electronic materials.

Theoretical Model To investigate the shot noise and differential conductance associated with the tunneling into Majorana modes on the surface of $\text{FeSe}_{0.45}\text{Te}_{0.55}$, we consider a two-dimensional 5-orbital model [27, 28] that was obtained from a fit to ARPES and STS experiments [28] and was recently proposed to explain the emergence of topological superconductivity in $\text{FeSe}_{0.45}\text{Te}_{0.55}$ as arising from the interplay between (i) a full superconducting s_{\pm} -

wave gap, (ii) surface magnetism, evidence for which was recently reported by ARPES [19] and quantum sensing [20] experiments, and (iii) a Rashba spin orbit (RSO) interaction that arises from the breaking of the inversion symmetry on the surface. The resulting Hamiltonian in real space is given by

$$\begin{aligned}
H_0 = & - \sum_{a,b=1}^5 \sum_{\mathbf{r},\mathbf{r}',\sigma} t_{\mathbf{r},\mathbf{r}'}^{ab} c_{\mathbf{r},a,\sigma}^\dagger c_{\mathbf{r}',b,\sigma} - \sum_{a=1}^5 \sum_{\mathbf{r},\sigma} \mu_{aa} c_{\mathbf{r},a,\sigma}^\dagger c_{\mathbf{r},a,\sigma} \\
& + i\alpha \sum_{a=1}^5 \sum_{\mathbf{r},\boldsymbol{\delta},\sigma,\sigma'} c_{\mathbf{r},a,\sigma}^\dagger (\boldsymbol{\delta} \times \boldsymbol{\sigma})_{\sigma\sigma'}^z c_{\mathbf{r}+\boldsymbol{\delta},a,\sigma'} \\
& - J \sum_{a=1}^5 \sum_{\mathbf{r},\sigma,\sigma'} \mathbf{S}_{\mathbf{r}} \cdot c_{\mathbf{r},a,\sigma}^\dagger \boldsymbol{\sigma}_{\sigma\sigma'} c_{\mathbf{r},a,\sigma'} \\
& + \sum_{a=1}^5 \sum_{\langle \mathbf{r},\mathbf{r}' \rangle} \Delta_{\mathbf{r}\mathbf{r}'}^{aa} c_{\mathbf{r},a,\uparrow}^\dagger c_{\mathbf{r}',a,\downarrow}^\dagger + \text{H.c.} \quad (1)
\end{aligned}$$

Here $a, b = 1, \dots, 5$ are the orbital indices corresponding to the d_{xz} -, d_{yz} -, $d_{x^2-y^2}$ -, d_{xy} -, and $d_{3z^2-r^2}$ -orbitals, respectively, $-t_{\mathbf{r}\mathbf{r}'}^{ab}$ represents the electronic hopping amplitude between orbital a at site \mathbf{r} and orbital b at site \mathbf{r}' on a two-dimensional square lattice, μ_{aa} is the on-site energy in orbital a , $c_{\mathbf{r},a,\sigma}^\dagger$ ($c_{\mathbf{r},a,\sigma}$) creates (annihilates) an electron with spin σ at site \mathbf{r} in orbital a , and $\boldsymbol{\sigma}$ is the vector of spin Pauli matrices. The superconducting order parameter $\Delta_{\mathbf{r}\mathbf{r}'}^{aa}$ represents intra-orbital pairing between next-nearest neighbor Fe sites \mathbf{r} and \mathbf{r}' (in the 1 Fe unit cell), yielding a superconducting s_{\pm} -wave symmetry [28]. Moreover, α represents the Rashba spin-orbit interaction arising from the breaking of the inversion symmetry at the surface [29] with $\boldsymbol{\delta}$ being the vector connecting nearest neighbor sites. $\mathbf{S}_{\mathbf{r}}$ denotes the ferromagnetically ordered moment [19, 20] which is locally exchanged coupled to the conduction electrons via an interaction J . The observation of ARPES experiments [19] are consistent with a considerable fraction of the ordered magnetic moment aligned perpendicular to the surface, such that we assume an out-of-plane ferromagnetic alignment of $\mathbf{S}_{\mathbf{r}}$ for concreteness. In the normal state, the Hamiltonian of Eq.(1) yields three Fermi surfaces in the 1Fe Brillouin zone whose orbital character implies that the superconducting order parameter is non-zero only in the d_{xz} -, d_{yz} -, and d_{xy} -orbitals [28]. Finally, as shown in Ref. [18], this model exhibits a series of topological phases that are characterized by the Chern number, C .

To compute the differential conductance and differential shot noise in a topological superconducting phase, we employ the Keldysh Greens function formalism, and obtain for the current flowing between the tip and the system

$$I(V) = \frac{2et_0}{h} \sum_{\sigma=\uparrow,\downarrow} \int_{-eV}^{eV} d\varepsilon \text{Re} [G_{ts}^<(\mathbf{r}, \sigma, \sigma, \varepsilon)] , \quad (2)$$

and for the zero-frequency shot-noise

$$\begin{aligned}
S(\omega = 0, V) = & \frac{2e^2 t_0^2}{h} \sum_{\sigma, \sigma'=\uparrow, \downarrow} \int_{-eV}^{eV} d\varepsilon \\
& \times [G_{tt}^>(\sigma, \sigma', \varepsilon) G_{ss}^<(\sigma', \sigma, \varepsilon) + G_{ss}^>(\sigma, \sigma', \varepsilon) G_{tt}^<(\sigma', \sigma, \varepsilon) \\
& + [F_{ss}^>(\sigma, \sigma', \varepsilon)]^* F_{tt}^<(\sigma', \sigma, \varepsilon) + [F_{tt}^>(\sigma, \sigma', \varepsilon)]^* F_{ss}^<(\sigma', \sigma, \varepsilon) \\
& - G_{ts}^>(\sigma, \sigma', \varepsilon) G_{ts}^<(\sigma', \sigma, \varepsilon) - G_{st}^>(\sigma, \sigma', \varepsilon) G_{st}^<(\sigma', \sigma, \varepsilon) \\
& - [F_{st}^>(\sigma, \sigma', \varepsilon)]^* F_{st}^<(\sigma', \sigma, \varepsilon) - [F_{ts}^>(\sigma, \sigma', \varepsilon)]^* F_{ts}^<(\sigma', \sigma, \varepsilon)] \quad (3)
\end{aligned}$$

Here, G, F are the normal and anomalous Greens functions, with t, s denoting the sites of the tip and the system between which electrons tunnel, and all Green's functions involving the system are evaluated at site \mathbf{r} and for orbital a [for details, see Supplemental Material (SM) Sec. 1]. dI/dV and dS/dV are then obtained by differentiating Eqs.(2) and (3), respectively.

Results There are three distinct cases in which Majorana modes emerge from the above described theoretical model for $\text{FeSe}_{0.45}\text{Te}_{0.55}$: chiral Majorana edge modes along domain walls, MZMs located in vortex cores, as well as MZMs located at the end of line defects [18]. We begin by studying the form of dS/dV and dI/dV for chiral Majorana edge modes that emerge at a domain wall separating a topological $C = 1$ region from a trivial $C = 0$ region. The observation of strong disorder in $\text{FeSe}_{0.45}\text{Te}_{0.55}$ [30, 31], combined with the fact that MZMs are not observed in all vortex cores, suggest that such domain walls could be realized on the surface of $\text{FeSe}_{0.45}\text{Te}_{0.55}$. In Fig. 1(a), we present the electronic dispersion as a function of momentum along the domain wall, showing two Majorana modes traversing the superconducting gap. We note that as we consider a system with periodic boundary conditions, the system considered here contains two domain walls, with a Chern number change of $\Delta C = 1$ at each of the domain walls, resulting in two Majorana modes, one located at each of the domain walls. In Fig. 1(b), we show a linecut of the local density of states (LDOS) across the domain wall: it shows an almost energy independent spectral weight inside the superconducting gap near the domain wall, arising from the chiral Majorana edge mode. In order to identify the universal features of the differential shot-noise and differential conductance associated with the tunneling into a single Majorana state of this chiral edge mode, however, we need to (a) resolve the Majorana states in energy, which can be done by considering a finite length of the domain wall, leading to discretized energy levels as revealed by the LDOS shown in Fig. 1(c), and (b) ensure that a finite lifetime of the Majorana states arises solely from its coupling to the tip. In Fig. 1(d), we present the voltage dependence of both dS/dV and dI/dV near the lowest energy Majorana state, for tunneling into the d_{xy} -orbital. Note that due to the finite size of the system we consider, the lowest energy Majorana

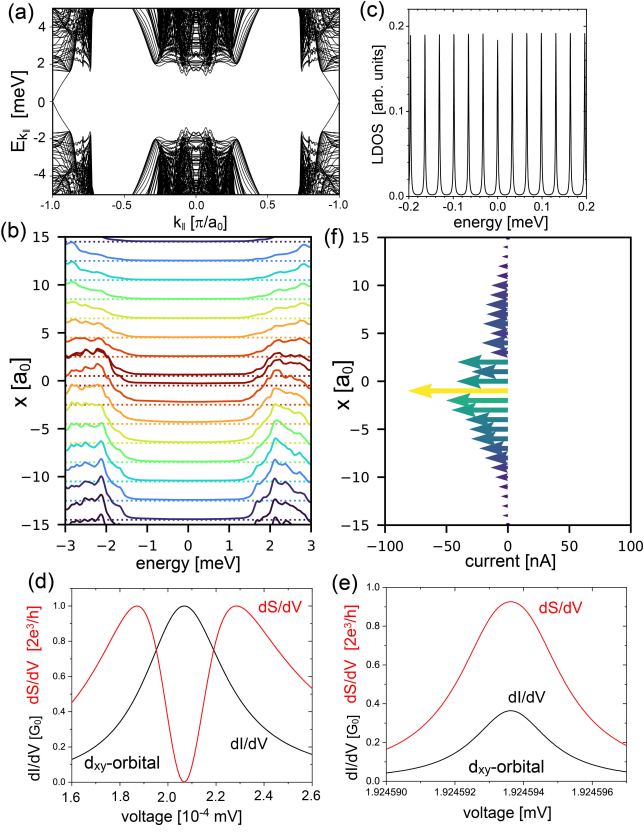


FIG. 1. Domain wall with $\alpha = 7$ meV separating a topological $C = 1$ regions with $J = 7.5$ meV from a trivial $C = 0$ region with $J = 0$. (a) Electronic dispersion as a function of momentum along the domain wall. The chiral Majorana edge mode traverses the superconducting gap. (b) LDOS along a linecut perpendicular to the domain wall. (c) Low energy LDOS in which individual Majorana states are energetically resolved. dS/dV (red line) and dI/dV (black line) for (d) the lowest energy Majorana state, and (e) for a state near the gap edge with $E = 1.9245$. (f) Spatial profile of the supercurrent near the domain wall.

Majorana state is located at a very small, but finite energy. As previously reported, we find that dI/dV reaches the quantum of conductance, G_0 , at the energy of the Majorana state [3], implying that at this energy, the transmission amplitude reaches unity. A qualitatively new feature of the Majorana modes is revealed by the differential shot noise, dS/dV , which vanishes at that bias where dI/dV reaches G_0 . The same result holds for tunneling into any of the other d -orbitals that possess spectral weight at the domain wall (see SM Sec. 2), implying that a quantized conductance and vanishing differential noise are universal features that are independent of the complex multi-orbital structure of a topological superconductor. We note that by defining a transmission amplitude $T(V)$ via $dI/dV = G_0 T(V)$, the differential shot noise obeys $dS/dV \sim T(V)[1 - T(V)]$ (see SM Sec. 2). A quantized dI/dV and vanishing dS/dV are also found

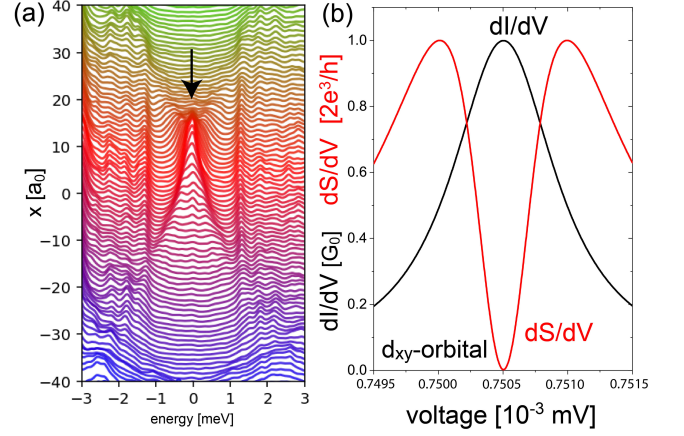


FIG. 2. (a) Linecut of the LDOS through the center of a vortex core in the topological $C = 1$ phase with $(\alpha, J) = (7, 8)$ meV for a uniform magnetic flux of 1 Wb, revealing the existence of a MZM. (b) dI/dV (black line) and dS/dV (red line) for tunneling into the MZM for the d_{xy} -orbital.

for higher energy Majorana states, until one approaches states near the gap edge. Indeed, for states close to the gap edge, we find significant deviations of dI/dV from G_0 , while dS/dV does not vanish any longer, as shown in Fig. 1(e). This demonstrates that both a quantized value for dI/dV and the vanishing of dS/dV are hallmarks of chiral Majorana edge modes. Concomitant with these results, we find that the domain wall carrying a chiral Majorana edge modes also gives rise to a non-vanishing supercurrent that flows parallel to the domain wall, as shown in Fig. 1(f). Such a supercurrent can be detected using an SSM scanned along the domain wall [26], such that the combination of dI/dV , dS/dV and SSM measurements can provide strong evidence for the existence of Majorana modes along a domain wall.

We next study the differential shot noise associated with the tunneling into a localized MZM in a vortex core by implementing the magnetic field via the Peierls substitution and compute the spatial dependence of the superconducting order parameters in the d_{xz} -, d_{yz} -, and d_{xy} -orbitals self-consistently (for details, see Ref. [18]). In Fig. 2(a) we plot a linecut of the LDOS through the center of the vortex core in the $C = 1$ phase, which reveals the existence of a MZM in its center (see black arrow). In Fig. 2(b), we present dS/dV and dI/dV , associated with the tunneling into this localized MZM. As expected, we again find that at the bias when dI/dV reaches the quantized quantum of conductance, dS/dV vanishes. As shown in SM Sec. 3, this results holds for tunneling into any of the d -orbitals, again supporting our conclusion that these results are universal and independent of any complex electronic bandstructure.

Finally, we consider the emergence of zero energy states at the end of line defects, recently observed in

monolayer $\text{FeSe}_{0.5}\text{Te}_{0.5}$ deposited on a SrTiO_3 substrate [15], whose spatial structure is similar to that expected for MZMs. It is presently unclear whether these MZMs are a characteristic feature of an underlying topological phase as argued in Ref. [18], similar to line defect MZMs predicted to occur in topological $p_x + ip_y$ -wave superconductors [32], or are independent of it, simply utilizing the monolayer's complex electronic structure to form a 1D topological superconductor as proposed in Refs.[15, 33, 34]. Indeed, it is presently unknown whether the $\text{FeSe}_{0.5}\text{Te}_{0.5}/\text{SrTiO}_3$ system itself is topological or not. While the mechanism proposed in Refs. [11, 17] requires a 3D bulk structure, and thus would not apply to this system, the mechanism described by Eq.(1) could give rise to topological superconductivity if $\text{FeSe}_{0.5}\text{Te}_{0.5}/\text{SrTiO}_3$ were also to exhibit ferromagnetism (which is presently unknown). Here, we follow the argumentation of Ref. [18], which has demonstrated that the emergence of MZMs at the end of line defects is a characteristic feature of the underlying topological phase. To study dS/dV and dI/dV associated with these line defect MZMs, we represent the line defect for simplicity as a line of potential scatterers (though magnetic scatterers could also be realized [33, 34]) described by the Hamiltonian

$$H_{def} = U_0 \sum_{a=1}^5 \sum_{\mathbf{R}, \sigma} c_{\mathbf{R}, a, \sigma}^\dagger c_{\mathbf{R}, a, \sigma}, \quad (4)$$

where U_0 is the potential scattering strength, and the sum runs over all sites \mathbf{R} of the line defect. As previously shown [18], when the underlying system is in a topological phase, there exist certain ranges of the scattering potential U_0 in which localized zero energy states emerge at the end of the line defect, whose spatial LDOS structure is consistent with that of MZMs, as shown in Fig. 3(a). In contrast, the next higher energy state is delocalized along the chain, as shown in Fig. 3(b). This qualitative difference between these two states is also reflected in the form of dI/dV and dS/dV . For tunneling into the lowest energy state, we again find that when dI/dV reaches G_0 , dS/dV vanishes, as shown in Fig. 3(c), establishing that this state is a MZM. This result holds for tunneling into all of the 5 Fe d -orbitals (see SM Sec. 4). In contrast, for the next higher energy state [see Fig. 3(d)], dI/dV does not reach G_0 , and dS/dV does not vanish, implying that this state is not topological in nature. Since dS/dV vanishes at the energy of a Majorana mode, a measurement of dS/dV can be employed to identify topological phase transitions. For example, consider the evolution of the lowest energy state, E_0 , associated with the line defect as a function of the scattering strength U_0 shown in Fig. 3(e). For those regions of U_0 with $E_0 = 0$ (shown with a gray background), we find that the differential shot noise for tunneling into the d_{yz} - and $d_{x^2-y^2}$ -orbitals also vanishes. In contrast, already for small deviations

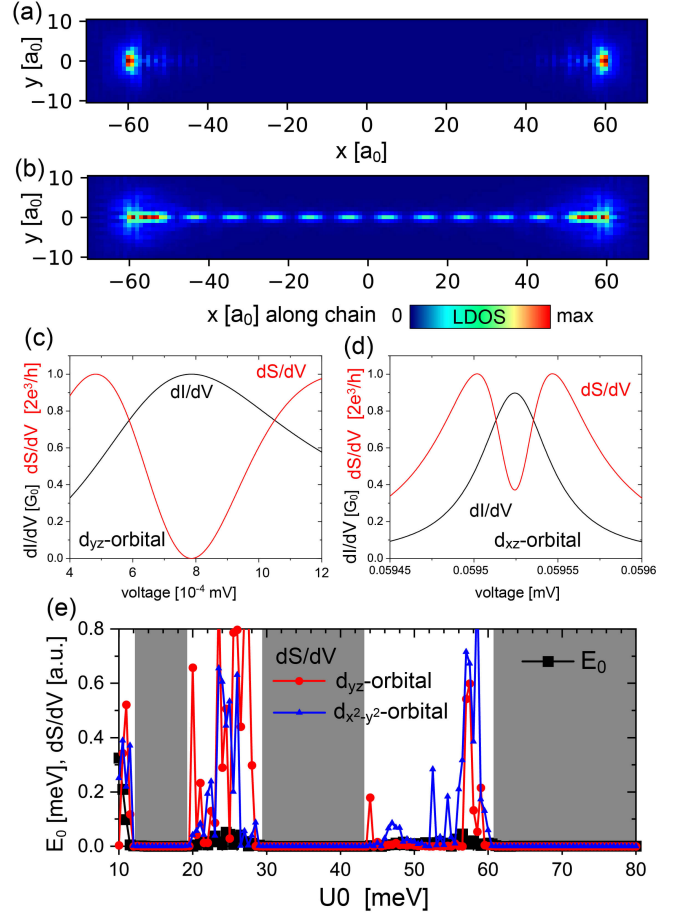


FIG. 3. Spatial structure of the LDOS around a line defect with $(\alpha, JS) = (7, 7.5)$ meV for (a) the lowest energy state at $E_0 = 0.000786$, and (b) the next higher energy state at $E_1 = 0.0595$. The line defect has a length is $L = 120a_0$ with scattering strength $U = 72.5$ meV. (c), (d) The respective dI/dV (black line) and dS/dV (red line) for tunneling into the d_{xy} -orbital near energies corresponding to panels (a) and (b), respectively. (e) The energy of the lowest energy state, as well as dS/dV for tunneling into the d_{xy} - and $d_{x^2-y^2}$ -orbitals, as a function of U_0 .

of E_0 from zero, on the order of 1% of the superconducting gap size, dS/dV exhibits significant deviations from zero, indicating that the lowest energy state is no longer topological. Thus, dS/dV represent a sensitive probe for the topological nature of very low energy states.

Conclusions In conclusion, we have studied the form of the differential noise, dS/dV , and the differential conductance, dI/dV , for tunneling into localized MZMs in vortex cores and at the end of line defects, and into chiral Majorana edge modes in $\text{FeSe}_{0.45}\text{Te}_{0.55}$. Using a 5-band model that was previously extracted from fits to ARPES and STS experiments [28], we demonstrated that for all three cases, when the differential conductance, dI/dV reaches the quantum of conductance, the differential shot-noise, dS/dV , as measured via scanning

tunneling shot noise spectroscopy, vanishes. In contrast, for low energy states that are trivial, dS/dV remains finite. These results demonstrate that dS/dV is a sensitive probe for the topological nature of low-energy states, being able to discriminate between topological and trivial low-energy states. This ability, in turn, can be employed to detect topological phase transitions. These results hold for tunneling into any of the Fe d -orbitals of $\text{FeSe}_{0.45}\text{Te}_{0.55}$, demonstrating that they are independent of the material's specific complex electronic bandstructure. In addition, we showed that a non-zero net supercurrent flows along domain walls separating topological and trivial regions. Thus, the combination of differential shot-noise, differential conductance, and measurements of local supercurrents via scanning probe microscopy techniques can provide a unique fingerprint for the existence of topological Majorana modes.

Acknowledgements

We would like to thank S. Rachel for stimulating discussions. The theoretical work on supercurrents and the differential conductance near domain walls was supported by the U. S. Department of Energy, Office of Science, Basic Energy Sciences, under Award No. DE-FG02-05ER46225 (E.M and D.K.M.). The theoretical work on the differential shot noise was supported by the Center for Quantum Sensing and Quantum Materials, an Energy Frontier Research Center funded by the U. S. Department of Energy, Office of Science, Basic Energy Sciences under Award DE-SC0021238 (K.H.W and D.K.M.). V.M and D.J.V.H acknowledge support by the Center for Quantum Sensing and Quantum Materials, an Energy Frontier Research Center funded by the U. S. Department of Energy, Office of Science, Basic Energy Sciences under Award DE-SC0021238.

-
- [1] K. T. Law, P. A. Lee, and T. K. Ng, Majorana Fermion Induced Resonant Andreev Reflection, *Phys. Rev. Lett.* **103**, 237001 (2009).
 - [2] K. Flensberg, Tunneling characteristics of a chain of Majorana bound states, *Phys. Rev. B* **82**, 180516 (2010).
 - [3] S. Rachel, E. Mascot, S. Cocklin, M. Vojta, and D. K. Morr, Quantized charge transport in chiral Majorana edge modes, *Phys. Rev. B* **96**, 205131 (2017).
 - [4] C. J. Bolech and E. Demler, Observing Majorana bound states in p-wave superconductors using noise measurements in tunneling experiments, *Phys. Rev. Lett.* **98**, 237002 (2007).
 - [5] B. Zocher and B. Rosenow, Modulation of Majorana-Induced Current Cross-Correlations by Quantum Dots, *Phys. Rev. Lett.* **111**, 036802 (2013).
 - [6] M. Diez, I. C. Fulga, D. I. Pikulin, J. Tworzydło, and C. W. J. Beenakker, Bimodal conductance distribution of Kitaev edge modes in topological superconductors, *New J. Phys.* **16**, 063049 (2014).
 - [7] D. E. Liu, M. Cheng, and R. M. Lutchyn, Probing Majorana physics in quantum-dot shot-noise experiments, *Phys. Rev. B* **91**, 081405 (2015).
 - [8] T. Jonckheere, J. Rech, A. Zazunov, R. Egger, A. Levy Yeyati, and T. Martin, Giant Shot Noise from Majorana Zero Modes in Topological Trijunctions, *Phys. Rev. Lett.* **122**, 097003 (2019).
 - [9] C. W. J. Beenakker and D. O. Oriekhov, Shot noise distinguishes Majorana fermions from vortices injected in the edge mode of a chiral p-wave superconductor, *SciPost Phys.* **9**, 080 (2020).
 - [10] V. Perrin, M. Civelli, and P. Simon, Discriminating majorana bound states by tunneling shot-noise tomography (2020), arXiv:2011.06893.
 - [11] P. Zhang, K. Yaji, T. Hashimoto, Y. Ota, T. Kondo, K. Okazaki, Z. Wang, J. Wen, G. D. Gu, H. Ding, and S. Shin, Observation of topological superconductivity on the surface of an iron-based superconductor, *Science* **360**, 182 (2018).
 - [12] D. Wang, L. Kong, P. Fan, H. Chen, S. Zhu, W. Liu, L. Cao, Y. Sun, S. Du, J. Schneeloch, R. Zhong, G. Gu, L. Fu, H. Ding, and H.-J. Gao, Evidence for Majorana bound states in an iron-based superconductor, *Science* **362**, 333 (2018).
 - [13] T. Machida, Y. Sun, S. Pyon, S. Takeda, Y. Kohsaka, T. Hanaguri, T. Sasagawa, and T. Tamegai, Zero-energy vortex bound state in the superconducting topological surface state of $\text{Fe}(\text{Se},\text{Te})$, *Nat. Mater.* **18**, 811 (2019).
 - [14] S. Zhu, L. Kong, L. Cao, H. Chen, M. Papaj, S. Du, Y. Xing, W. Liu, D. Wang, C. Shen, F. Yang, J. Schneeloch, R. Zhong, G. Gu, L. Fu, Y.-Y. Zhang, H. Ding, and H.-J. Gao, Nearly quantized conductance plateau of vortex zero mode in an iron-based superconductor, *Science* **367**, 189 (2020).
 - [15] C. Chen, K. Jiang, Y. Zhang, C. Liu, Y. Liu, Z. Wang, and J. Wang, Atomic line defects and zero-energy end states in monolayer $\text{Fe}(\text{Te},\text{Se})$ high-temperature superconductors, *Nat. Phys.* **16**, 536 (2020).
 - [16] Z. Wang, J. O. Rodriguez, L. Jiao, S. Howard, M. Graham, G. D. Gu, T. L. Hughes, D. K. Morr, and V. Madhavan, Evidence for dispersing 1D Majorana channels in an iron-based superconductor, *Science* **367**, 104 (2020).
 - [17] Z. Wang, P. Zhang, G. Xu, L. K. Zeng, H. Miao, X. Xu, T. Qian, H. Weng, P. Richard, A. V. Fedorov, H. Ding, X. Dai, and Z. Fang, Topological nature of the $\text{FeSe}_{0.5}\text{Te}_{0.5}$ superconductor, *Phys. Rev. B* **92**, 115119 (2015).
 - [18] E. Mascot, S. Cocklin, M. Graham, M. Mashkooi, S. Rachel, and D. K. Morr, Topological Surface Superconductivity in $\text{FeSe}_{0.45}\text{Te}_{0.55}$, arXiv:2102.05116.
 - [19] N. Zaki, G. Gu, A. Tsvetlik, C. Wu, and P. D. Johnson, Time-reversal symmetry breaking in the Fe-chalcogenide superconductors, *Proc. Natl. Acad. Sci. U.S.A.* **118**, e2007241118 (2021).
 - [20] N. J. McLaughlin, H. Wang, M. Huang, E. Lee-Wong, L. Hu, H. Lu, G. Yan, G. Gu, C. Wu, Y.-Z. You, and C. Du, Observation of Superconductivity Induced Ferromagnetism in an Fe-Chalcogenide Superconductor, arXiv:2106.15882.
 - [21] H. Birk, M. Dejong, and C. Schonenberger, Shot-noise suppression in the single-electron tunneling regime, *Phys. Rev. Lett.* **75**, 1610 (1995).
 - [22] U. Kemiktarak, T. Ndukum, K. C. Schwab, and K. L. Ekinci, Radio-frequency scanning tunnelling microscopy, *Nature* **450**, 85 (2007).
 - [23] M. Herz, S. Bouvron, E. Cavar, M. Fonin, W. Belzig, and

- E. Scheer, Fundamental quantum noise mapping with tunnelling microscopes tested at surface structures of subatomic lateral size, *Nanoscale* **5**, 9978 (2013).
- [24] K. M. Bastiaans, D. Cho, T. Benschop, I. Battisti, Y. Huang, M. S. Golden, Q. Dong, Y. Jin, J. Zaanen, and M. P. Allan, Charge trapping and super-Poissonian noise centres in a cuprate superconductor, *Nat. Phys.* **14**, 1183 (2018).
- [25] F. Massee, Y. K. Huang, M. S. Golden, and M. Aprili, Noisy defects in the high-T-c superconductor $\text{Bi}_2\text{Sr}_2\text{CaCu}_2\text{O}_{8+x}$, *Nat. Commun.* **10**, 544 (2019).
- [26] E. M. Spanton, K. C. Nowack, L. Du, G. Sullivan, R.-R. Du, and K. A. Moler, Images of edge current in InAs/GaSb quantum wells, *Phys. Rev. Lett.* **113**, 026804 (2014).
- [27] S. Graser, T. A. Maier, P. J. Hirschfeld, and D. J. Scalapino, Near-degeneracy of several pairing channels in multiorbital models for the Fe pnictides, *New J. Phys.* **11**, 025016 (2009).
- [28] S. Sarkar, J. Van Dyke, P. O. Sprau, F. Massee, U. Welp, W.-K. Kwok, J. C. S. Davis, and D. K. Morr, Orbital superconductivity, defects, and pinned nematic fluctuations in the doped iron chalcogenide $\text{FeSe}_{0.45}\text{Te}_{0.55}$, *Phys. Rev. B* **96**, 060504 (2017).
- [29] S. Nadj-Perge, I. K. Drozdov, J. Li, H. Chen, S. Jeon, J. Seo, A. H. MacDonald, B. A. Bernevig, and A. Yazdani, Observation of Majorana fermions in ferromagnetic atomic chains on a superconductor, *Science* **346**, 602 (2014).
- [30] D. Cho, K. M. Bastiaans, D. Chatzopoulos, G. D. Gu, and M. P. Allan, A strongly inhomogeneous superfluid in an iron-based superconductor, *Nature* **571**, 541 (2019).
- [31] D. Wang, R. Zhong, G. Gu, and R. Wiesendanger, Surface orbital order and chemical potential inhomogeneity of the iron-based superconductor $\text{FeTe}_{0.55}\text{Se}_{0.45}$ investigated with special STM tips, arXiv:2104.07418.
- [32] M. Wimmer, A. R. Akhmerov, M. V. Medvedyeva, J. Tworzydło, and C. W. J. Beenakker, Majorana bound states without vortices in topological superconductors with electrostatic defects, *Phys. Rev. Lett.* **105**, 046803 (2010).
- [33] Y. Zhang, K. Jiang, F. Zhang, J. Wang, and Z. Wang, Atomic line defects and topological superconductivity in unconventional superconductors, *Phys. Rev. X* **11**, 011041 (2021).
- [34] X. Wu, J.-X. Yin, C.-X. Liu, and J. Hu, Topological magnetic line defects in $\text{Fe}(\text{Te},\text{Se})$ high-temperature superconductors, arXiv:2004.05848.

Supplemental Material for Shot-noise and differential conductance as signatures of putative topological superconductivity in $\text{FeSe}_{0.45}\text{Te}_{0.55}$

Ka Ho Wong¹, Eric Mascot¹, Vidya Madhavan², Dale J. Van Harlingen², and Dirk K. Morr¹

¹ *University of Illinois at Chicago, Chicago, IL 60607, USA*

² *University of Illinois at Urbana Champaign, Champaign, IL 61801, USA*

I. THEORETICAL FORMALISM

To investigate the differential conductance, dI/dV , and the differential noise, dS/dV for tunneling into Majorana modes, we consider the Hamiltonian that was proposed in Ref.[?] to explain the emergence of topological surface superconductivity in $\text{FeSe}_{0.45}\text{Te}_{0.55}$. To compute dI/dV and dS/dV , we need to a term, H_t to the Hamiltonian that describes the electron tunneling from the STS tip into the system. The total Hamiltonian in real space is then given by $H = H_0 + H_{tip}$, where

$$\begin{aligned}
 H_0 = & - \sum_{a,b=1}^5 \sum_{\mathbf{r},\mathbf{r}',\sigma} t_{\mathbf{r},\mathbf{r}'}^{ab} c_{\mathbf{r},a,\sigma}^\dagger c_{\mathbf{r}',b,\sigma} - \sum_{a=1}^5 \sum_{\mathbf{r},\sigma} \mu_{aa} c_{\mathbf{r},a,\sigma}^\dagger c_{\mathbf{r},a,\sigma} \\
 & + i\alpha \sum_{a=1}^5 \sum_{\mathbf{r},\delta,\sigma,\sigma'} c_{\mathbf{r},a,\sigma}^\dagger (\boldsymbol{\delta} \times \boldsymbol{\sigma})_{\sigma\sigma'}^z c_{\mathbf{r}+\delta,a,\sigma'} + J \sum_{a=1}^5 \sum_{\mathbf{r},\sigma,\sigma'} \mathbf{S}_{\mathbf{r}} \cdot c_{\mathbf{r},a,\sigma}^\dagger \boldsymbol{\sigma}_{\sigma\sigma'} c_{\mathbf{r},a,\sigma'} \\
 & + \sum_{a=1}^5 \sum_{\langle \mathbf{r},\mathbf{r}' \rangle} \Delta_{\mathbf{r}\mathbf{r}'}^{aa} c_{\mathbf{r},a,\uparrow}^\dagger c_{\mathbf{r}',a,\downarrow}^\dagger + \text{H.c.} \\
 H_t = & -t_0 \sum_{\sigma} (c_{\mathbf{r},a,\sigma}^\dagger d_{\sigma} + \text{H.c.})
 \end{aligned} \tag{S1}$$

Here $a, b = 1, \dots, 5$ are the orbital indices corresponding to the d_{xz} -, d_{yz} -, $d_{x^2-y^2}$ -, d_{xy} -, and $d_{3z^2-r^2}$ -orbitals, respectively, $-t_{\mathbf{r}\mathbf{r}'}^{ab}$ represents the electronic hopping amplitude between orbital a at site \mathbf{r} and orbital b at site \mathbf{r}' on a two-dimensional square lattice, μ_{aa} is the on-site energy in orbital a , $c_{\mathbf{r},a,\sigma}^\dagger (c_{\mathbf{r},a,\sigma})$ creates (annihilates) an electron with spin σ at site \mathbf{r} in orbital a , and $\boldsymbol{\sigma}$ is the vector of spin Pauli matrices. The superconducting order parameter $\Delta_{\mathbf{r}\mathbf{r}'}^{aa}$ represents intra-orbital pairing between next-nearest neighbor Fe sites \mathbf{r} and \mathbf{r}' (in the 1 Fe unit cell), yielding a superconducting s_{\pm} -wave symmetry [?]. Moreover, α denotes the Rashba spin-orbit interaction arising from the breaking of the inversion symmetry at the surface[?] with $\boldsymbol{\delta}$ being the vector connecting nearest neighbor sites. Moreover, $-t_0$ represents the tunneling elements for electron tunneling from the STS tip into orbital a at site \mathbf{r} .

To compute dI/dV and dS/dV , we need to find the Greens functions of the entire system, superconductor plus STS tip. To this end, we introduce the following spinor for the superconductor

$$\begin{aligned}
 \Psi^\dagger &= (\psi_1^\dagger, \psi_2^\dagger, \dots, \psi_N^\dagger) \\
 \psi_p^\dagger &= (\psi_{p,\uparrow}^\dagger, \psi_{p,\downarrow}^\dagger, \psi_{p,\downarrow}^T, -\psi_{p,\uparrow}^T) \\
 \psi_{p,\sigma}^\dagger &= (c_{p,\sigma,xz}^\dagger, c_{p,\sigma,yz}^\dagger, c_{p,\sigma,x^2-y^2}^\dagger, c_{p,\sigma,xy}^\dagger, c_{p,\sigma,3z^2-r^2}^\dagger)
 \end{aligned} \tag{S2}$$

where $1, 2, \dots$ denotes a site in the system, with $N = N_x \times N_y$ being the total number of sites. The Hamiltonian H_0 in Eq.(S1) can then be written in the form

$$H_0 = \Psi^\dagger \hat{H}_0 \Psi \tag{S3}$$

and we can define the Greens function matrix of the superconductor (decoupled from the STS tip) in Matsubara time via

$$\hat{g}_{sc}(\tau) = -\langle \mathcal{T}_\tau \Psi(\tau) \Psi^\dagger(0) \rangle. \tag{S4}$$

yielding for \hat{g}_{sc} in Matsubara frequency space

$$\hat{g}_{sc}(i\omega_n) = \left[i\omega_n \hat{1} - \hat{H}_0 \right]^{-1}. \tag{S5}$$

Similarly, we can define the Greens function of the tip in Matsubara time via

$$\hat{g}_{\text{tip}}(\tau) = -\langle \mathcal{T}_\tau \phi(\tau) \phi^\dagger(0) \rangle \quad (\text{S6})$$

where

$$\phi^\dagger = (d_\uparrow^\dagger, d_\downarrow^\dagger, d_\downarrow, -d_\uparrow) \quad (\text{S7})$$

Next, we employ the Dyson equation to include the tunneling between the STS tip and the superconductor, yielding the full Greens function of the entire system via

$$\begin{aligned} G^{<, >}(\omega) &= [\hat{1} - \hat{g}^r(\omega) \hat{H}_t]^{-1} \hat{g}^{<, >}(\omega) [\hat{1} - \hat{H}_t \hat{g}^a(\omega)]^{-1} \\ G^{r, a}(\omega) &= [(\hat{g}^{r, a}(\omega))^{-1} - \hat{H}_t]^{-1} \end{aligned} \quad (\text{S8})$$

where, with $x = <, >, r, a$

$$\hat{g}^x(\omega) = \begin{pmatrix} \hat{g}_{\text{tip}}^x(\omega) & 0 \\ 0 & \hat{g}_{\text{sc}}^x(\omega) \end{pmatrix} \quad (\text{S9})$$

$\hat{g}_{\text{sc}}^{r, a}(\omega)$ are the retarded and advanced forms of Eq.(S5), and $\hat{g}_{\text{sc}}^<(\omega)$ is the lesser Greens function matrix given by

$$\hat{g}_{\text{sc}}^<(\omega) = -n_F(\omega)(\hat{g}_{\text{sc}}^r(\omega) - \hat{g}_{\text{sc}}^a(\omega)) \quad (\text{S10})$$

where $n_F(\omega)$ is the Fermi distribution function. For the tip, we consider the wide-band limit, such that

$$\begin{aligned} \hat{g}_{\text{tip}}^{r, a} &= \mp i\pi N_0 \hat{1} \\ \hat{g}_{\text{tip}}^< &= i\pi N_0 \begin{pmatrix} n_F(\omega - eV) & 0 & 0 & 0 \\ 0 & n_F(\omega - eV) & 0 & 0 \\ 0 & 0 & n_F(\omega + eV) & 0 \\ 0 & 0 & 0 & n_F(\omega + eV) \end{pmatrix} \end{aligned} \quad (\text{S11})$$

where e is the electron charge, and V is the potential difference between the tip and the grounded superconductor. Moreover, using the expanded spinor

$$\bar{\Psi}^\dagger = (\phi, \psi_1^\dagger, \psi_2^\dagger, \dots, \psi_N^\dagger) \quad (\text{S12})$$

we can rewrite H_t as

$$H_t = \bar{\Psi}^\dagger \hat{H}_t \bar{\Psi} \quad (\text{S13})$$

which defines \hat{H}_t in Eq.(S8).

The current flowing between the STS tip and the superconductor is given by [?]]

$$I(V) = \frac{2et_0}{h} \sum_{\sigma=\uparrow, \downarrow} \int_{-eV}^{eV} d\varepsilon \text{Re} [G_{dc}^<(\mathbf{r}, \sigma, \sigma, \varepsilon)] \quad (\text{S14})$$

where $\omega = eV/\hbar$. The zero-frequency shot-noise for tunneling into orbital a at site \mathbf{r} is defined as the current-current correlation function in real time

$$S(\mathbf{r}, a, t, t') = \langle \{ \hat{I}_a(\mathbf{r}, t) - I_a(\mathbf{r}), \hat{I}_a(\mathbf{r}, t') - I_a(\mathbf{r}) \} \rangle \quad (\text{S15})$$

where \hat{I}_a is the current operator, and $I_a(\mathbf{r})$ is the steady-state current that flows from the tip into orbital a at site \mathbf{r} . We then obtain

$$\begin{aligned} S_0(\mathbf{r}, a, \omega = 0) &= \frac{2e^2 t_0^2}{h} \sum_{\sigma, \sigma'=\uparrow, \downarrow} \int_{-eV}^{eV} d\varepsilon [G_{tt}^>(\sigma; \sigma', \varepsilon) G_{ss}^<(\mathbf{r}, a, \sigma', \sigma, \varepsilon) + G_{cc}^>(\mathbf{r}, a, \sigma, \sigma', \varepsilon) G_{dd}^<(\sigma', \sigma, \varepsilon) \\ &+ [F_{cc}^>(\mathbf{r}, a, \sigma, \sigma', \varepsilon)]^* F_{dd}^<(\sigma', \sigma, \varepsilon) + [F_{dd}^>(\sigma, \sigma', \varepsilon)]^* F_{cc}^<(\mathbf{r}, a, \sigma', \sigma, \varepsilon) \\ &- G_{dc}^>(\mathbf{r}, a, \sigma, \sigma', \varepsilon) G_{dc}^<(\mathbf{r}, a, \sigma', \sigma, \varepsilon) - G_{cd}^>(\mathbf{r}, a, \sigma, \sigma', \varepsilon) G_{cd}^<(\mathbf{r}, a, \sigma', \sigma, \varepsilon) \\ &- [F_{cd}^>(\mathbf{r}, a, \sigma, \sigma', \varepsilon)]^* F_{cd}^<(\mathbf{r}, a, \sigma', \sigma, \varepsilon) - [F_{dc}^>(\mathbf{r}, a, \sigma, \sigma', \varepsilon)]^* F_{dc}^<(\mathbf{r}, a, \sigma', \sigma, \varepsilon)] . \end{aligned} \quad (\text{S16})$$

All Greens function in Eqs.(S14) and (S16) are elements of the Greens function matrices given in Eq.(S8), with G and F corresponding to the normal and anomalous Greens functions, t, s denoting the tip and the system, and all Green's functions involving the system are evaluated at site \mathbf{r} and for orbital a . For example, $G_{dc}^<(\mathbf{r}, a, \sigma', \sigma, \varepsilon)$ is the lesser form of the Greens function in Matsubara time given by

$$G_{dc}(\sigma'; \mathbf{r}, a, \sigma, \tau) = -\langle \mathcal{T}_\tau d_{\sigma'}(\tau) c_{\mathbf{r}, a, \sigma}^\dagger(0) \rangle \quad (\text{S17})$$

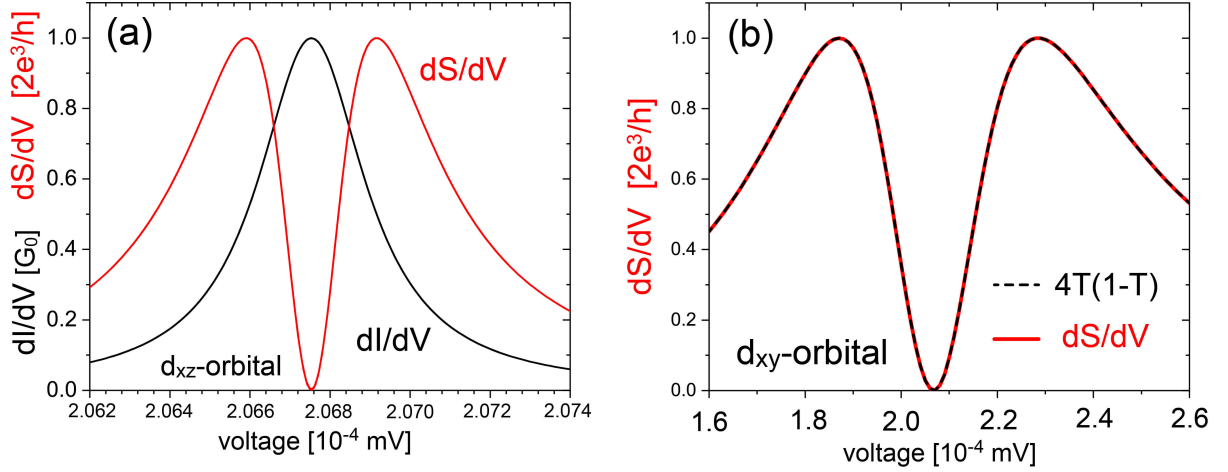


FIG. S1. Domain wall for $\alpha = 7$ meV separating a topological $C = 1$ regions with $J = 7.5$ meV from a trivial $C = 0$ region with $J = 0$. (a) dS/dV and dI/dV for the lowest energy Majorana state for tunneling into the d_{xz} -orbital. (b) Comparison of dS/dV (red line) and $T(V)[1 - T(V)]$ (dashed black line) for the lowest energy Majorana state and tunneling into the d_{xy} -orbital.

II. dS/dV AND dI/dV FOR TUNNELING INTO A CHIRAL MAJORANA EDGE MODE

For the domain wall discussed in Fig. 1 of the main text, only the d_{xy} - and d_{xz} -orbitals possess a non-vanishing spectral weight near zero energy at the location of the domain wall. The resulting dI/dV and dS/dV for tunneling into the d_{xy} -orbital are shown in Fig. 1(d) of the main text, while those for tunneling into the d_{xz} -orbital are shown in Fig. S1(a). Similar to the results shown in Fig. 1(d), we find that dS/dV vanishes when dI/dV reaches G_0 . Since the spectral weight of the d_{xz} -orbital is significantly smaller than that of the d_{xy} -orbital at the domain wall, we find that the energy width of dI/dV for the d_{xz} -orbital is significantly smaller than that of the d_{xy} -orbital. The spectral weight of the chiral Majorana modes in the remaining three orbitals is vanishingly small at the domain wall, such that they are not considered here.

To demonstrate the relation between dI/dV and dS/dV , we write

$$\frac{dI(V)}{dV} = G_0 T(V) \quad (\text{S18})$$

where $T(V)$ is the bias-dependent transmission coefficient. We then find that dS/dV can be written as

$$\frac{dS(V)}{dV} = \frac{8e^3}{h} T(V)[1 - T(V)] \quad (\text{S19})$$

In Fig. S2(b), we plot dS/dV (in units of $2e^3/h$) together with $T(V)[1 - T(V)]$, as extracted from Eq.(S18). The very good agreement between these two results demonstrates the functional relationship between dI/dV and dS/dV shown in Eqs.(S18) and (S19).

III. dS/dV AND dI/dV FOR TUNNELING INTO A LOCALIZED MZM IN A VORTEX CORE

dS/dV and dI/dV for tunneling into the d_{xy} -orbital of a localized MZM in a vortex core was shown in Fig. 2 of the main text. In Fig. S2, we present dS/dV and dI/dV for tunneling into the four remaining orbitals. In each case, we find that dS/dV vanishes when dI/dV reaches the quantum of conductance, G_0 . This result demonstrates that the vanishing of dS/dV is independent of the complex electronic structure of $\text{FeSe}_{0.45}\text{Te}_{0.55}$.

IV. dS/dV AND dI/dV FOR TUNNELING INTO A LOCALIZED MZM AT THE END OF A LINE DEFECT

dS/dV and dI/dV for tunneling into the d_{xz} -orbital of a localized MZM at the end of a line defect was shown in Fig. 3(c) of the main text. Similar to those results, we find that for tunneling into the four remaining orbitals (see Fig. S3), dS/dV vanishes when dI/dV reaches the quantum of conductance.

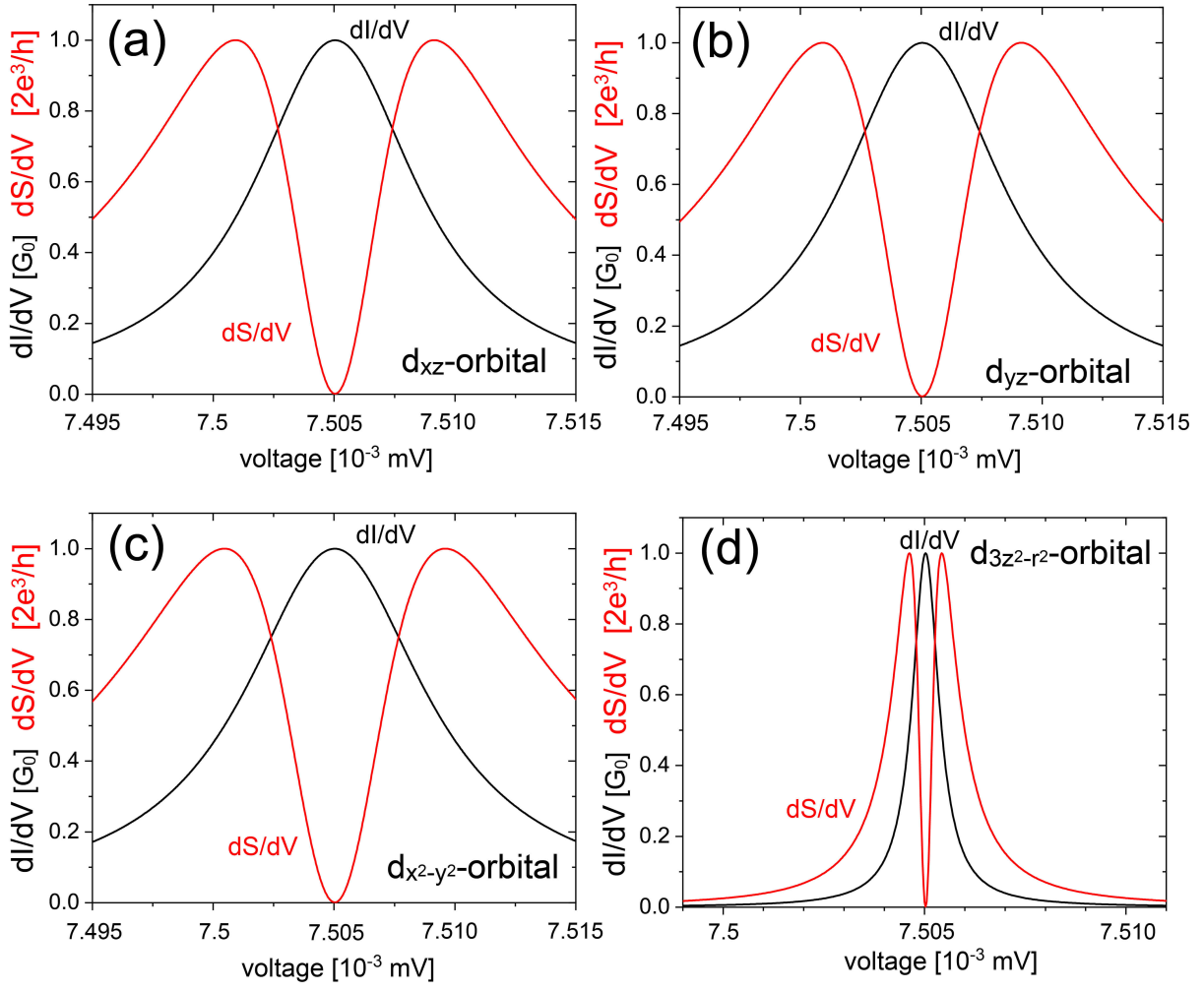


FIG. S2. dS/dV and dI/dV for the lowest energy Majorana state for tunneling into the (a) d_{xz} -orbital, (b) d_{yz} -orbital, (c) $d_{x^2-y^2}$ -orbital, and (d) $d_{3z^2-r^2}$ -orbital of a MZM located at the center of a vortex core in the topological $C = 1$ phase with $(\alpha, J) = (7, 8)$ meV for a uniform magnetic flux of 1 Wb.

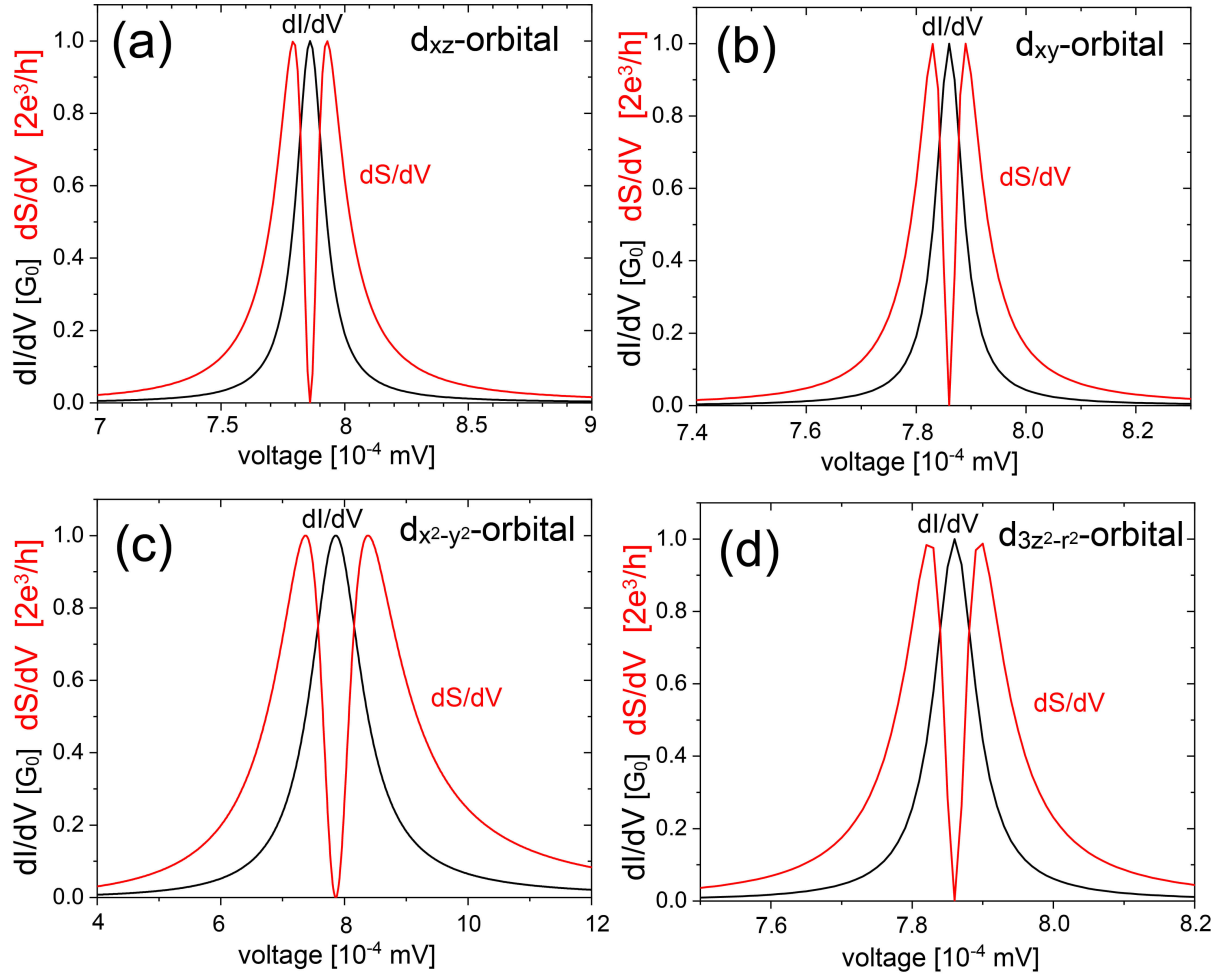


FIG. S3. dS/dV and dI/dV for the lowest energy Majorana state for tunneling into the (a) d_{xz} -orbital, (b) d_{xy} -orbital, (c) $d_{x^2-y^2}$ -orbital, and (d) $d_{3z^2-r^2}$ -orbital of a MZM located at the end of a line defect of length $L = 120a_0$ with $(\alpha, JS) = (7, 7.5)$ meV.